Biomass and Bioenergy 125 (2019) 204–211

Contents lists available at ScienceDirect

Biomass and Bioenergy

journal homepage: www.elsevier.com/locate/biombioe

A decentralized biomass torrefaction reactor concept. Part II: Mathematical model and scaling law

Kevin S. Kung[a,b,c,*], Ahmed F. Ghoniem[a,b]

[a] Department of Mechanical Engineering, MIT, Cambridge, MA, USA
[b] Tata Center for Technology and Design, MIT, Cambridge, MA, USA
[c] Department of Biological Engineering, MIT, Cambridge, MA, USA

ARTICLE INFO

Keywords:
Biomass
Torrefaction
Reactor design
Multi-scale modeling

ABSTRACT

In Part I of the study, we proposed a simplified biomass torrefaction moving bed reactor design capable of decentralized, small-scale, and mobile deployment operated under an oxygen-lean condition. We built and validated a laboratory-scale test reactor. In the present study, we develop a mathematical description of the reactor and show that it produces reasonable fit to our experimental data. Contrary to many existing biomass gasifier studies, we demonstrate that at the small test-reactor scale, heat loss mechanism through the side wall is significant and cannot be ignored in the modeling. We further demonstrated that at the small test-reactor scale, the rapid axial thermal conduction plays a role in the heat transfer within the moving bed. Furthermore, by interrogating the scaling behaviors of the reactor, we show that as we scale up our current laboratory-scale reactor, at the same torrefaction severity, the mass yield of the torrefied biomass is predicted to increase by 10–20%, due to the decrease in relative heat losses at a larger scale. This study, therefore, seeks to understand and quantify some of the limitations of testing a scaled-down reactor prototype. The understanding gained in this study can both inform scaling laws for at-scale reactor designs, as well as point out areas of future work in order to develop a higher-fidelity description.

1. Introduction

In Part I of this two-part study [24], we described a novel, simplified design concept for small-to medium-scale applications that operates under oxygen-lean conditions. As shown in Fig. 1, reproduced from Part I of the study, the reactor consists of a moving bed, in which the input raw biomass migrates downwards by gravity and is continuously removed by an auger at the bottom, and in which air, which is injected at the bottom of the moving bed at room temperature, undergoes limited reaction with the biomass phase before migrating upwards in a countercurrent manner, heating the biomass up in the moving bed [1]. In the previous study, we carried out a multi-scale analysis to understand the major chemical and heat transfer forces at play at different scales within the reactor, and then proceeded to design and test a laboratory-scale reactor that provided initial validation of our concept. From our experimental set-up, we demonstrated that this reactor indeed could be operated stably under various conditions to produce outputs consistent with biomass torrefaction. From our multi-scale analysis, we showed that in this reactor, heat transfer within the reactor is driven mainly by advective effects, and that heat loss effects, contrary to some recent studies, cannot generally be neglected in a small test reactor.

In this Part II of the study, we develop this reactor concept further by further exploring and quantifying the results from our multi-scale analysis. We describe a more detailed mathematical model description of the reactor, fit it to our experimental data, and demonstrate what we can learn in terms of the finer details of reactor behaviors as well as some relevant scaling strategies.

In developing a suitable mathematical model for our biomass torrefaction reactor concept, we first look to the existing literature for similar countercurrent moving bed reactor designs for a related thermochemical process of biomass gasification [2–9], as well as a few models describing other biomass torrefaction reactor designs [10,11]. While some aspects of chemistry and heat transfer within the reactor will be different for the gasification and the torrefaction regimes, we also strive to learn as much as possible from the gasifier models.

DOI of original article: https://doi.org/10.1016/j.biombioe.2018.11.004
* Corresponding author. Room 3-339, 77 Massachusetts Avenue, Cambridge, MA, 02139, USA.
E-mail address: kkung@mit.edu (K.S. Kung).

https://doi.org/10.1016/j.biombioe.2018.12.001

Available online 19 December 2018
0961-9534/

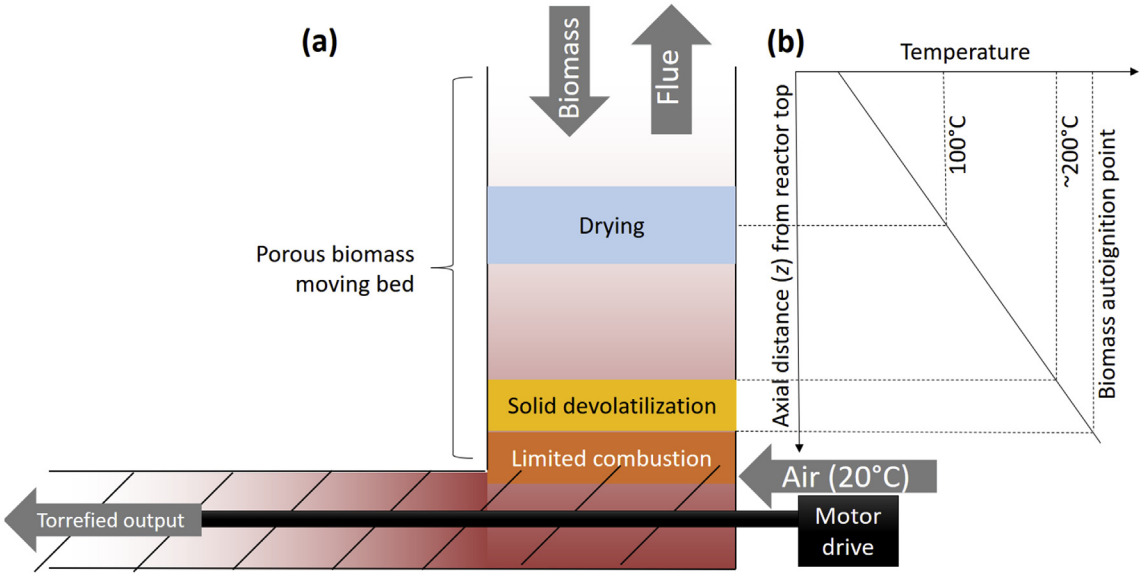

Fig. 1. A reproduction of the same figure from Part I of this study, showing (a) a schematic of an oxygen-lean moving bed torrefaction reactor design, and (b) guessed axial temperature profile and behaviors within the reactor.

2. Problem formulation

We start with a one-dimensional model of the reactor in the axial direction (z). While we expect there to be radial temperature gradients in addition to axial temperature gradients, for now, we choose to study the axial temperature profile because (a) it is more interesting for the purpose of torrefaction, and (b) our experimental set-up currently only possesses the ability to measure and verify the axial temperature profile. As defined in Fig. 2, the top of the reactor has position $z = 0$, while the bottom of the reactor, $z = L_r$. The inner radius of the moving bed reactor is denoted by R_r. The surrounding reactor wall, comprising of stainless steel 304, has a thickness $R_m - R_r$. Furthermore, surrounding the reactor wall, a ceramic-based insulation has a thickness $R_w - R_m$. For now, we ignore the modeling of any transient behaviors of the reactor, as we are mostly interested in its steady-state status. With these assumptions in mind, the main processes that we will model include:

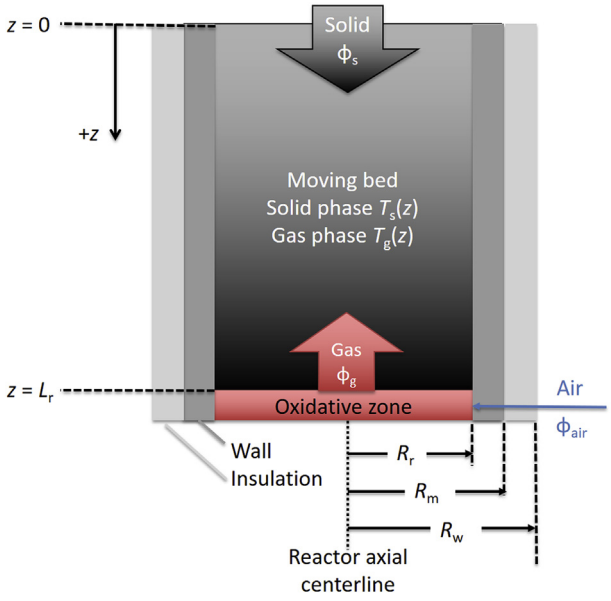

Fig. 2. A schematic representation of the modeling coordinates in the reactor.

1. Mass flux profile of the solid species
2. Mass flux profile of bound moisture
3. Overall elemental composition of the solid species
4. Temperature profile of the solid phase
5. Temperature profile of the gas phase
6. Temperature profile of the reactor wall

There are two major differences between what our model captures versus what existing biomass gasifier models capture. Firstly, unlike the existing gasifier models, our model carries out a detailed account of the temperature profile of the reactor wall. As we demonstrated in Part I, due to the small size of our laboratory-scale reactor, heat loss through the side wall becomes a significant process, and we would like this particular feature captured in detail. As we will show later, the metallic reactor wall has a much higher axial thermal conductivity compared to either the gas and solid phase within the reactor, and this itself could play a non-trivial role in redistributing the heat axially within the reactor. Secondly, in our modeling approach, we are much more interested in the solid species evolution rather than that of the gas/volatile species, as biomass torrefaction seeks to quantify and maximize the utility of the solid species. Indeed, unlike traditional gasifier modeling, the current biomass literature lacks a comprehensive understanding of the gas-phase kinetics in an oxygen-lean torrefaction regime. Therefore, as we will describe later, we describe the combustion of biomass and/or volatile in a lump-sum treatment that prevents us from obtaining a detailed species-by-species mass balance of the gases. Indeed, as shown in Fig. 2, except for the very thin "oxidative zone" at the very bottom of the reactor, we assume that throughout the rest of the moving bed, there is little or no gas-phase reaction, and the only chemistry that occurs relates to solid-phase devolatilization. This assumption is likely inaccurate, and can be refined in further studies.

Finally, as justified by the dimensional analysis in Part I, we assume that in the moving bed design, the biomass particles are thermally thin. Therefore, the model below ignores any intraparticle thermal gradients. This may not be generally true for thick particles (thickness $>$ 1 cm), and in future studies we can incorporate more detailed intraparticle treatment.

2.1. Constitutive equations

With these assumptions in mind, we can write the axial

conservation equations in the domain of the biomass moving bed ($0 \le z \le L_r$) as:

- Mass fluxes of four solid-phase pseudospecies (A which is also raw biomass, torrefied solid B, torrefied solid C, and bound moisture) as well as three gas/volatile species (volatile V1, volatile V2, and unbound moisture) to be defined in the chemical submodel below:

$$\frac{d\Phi_i}{dz} = r_i,$$

where Φ_i is the mass flux through the reactor cross-section of the ith species, and r_i is the volumetric creation rate [kg s^{-1} m^{-3}] of the ith species and is calculated in the coupled chemical kinetics/thermochemistry submodel. Note that, as done in other similar studies on biomass moving bed [3,4,10], we have assumed that diffusion of the gas species is negligible compared to convection. It is understood that the mass flux of the dry solid through the reactor is $\Phi_s = \Phi_A + \Phi_B + \Phi_C + \Phi_M$.

- Elemental composition of the solid species comprising of carbon, hydrogen, oxygen, nitrogen, and ash:

$$\frac{d}{dz}(\Phi_s Y_j) = \sum_i r_i Y_{ij},$$

where Y_j is the mass fraction of the jth elemental component, and Y_{ij} is the mass fraction of the jth elemental component in the ith solid pseudospecies.

- Solid-phase steady-state energy conservation:

$$\frac{d}{dz}(\Phi_s c_{p,s} T_s) = \frac{d}{dz}\left(k_s \frac{dT_s}{dz}\right) - \sum_i r_i H_i - q_{sg} - q_{sw}.$$

Here, $c_{p,s}$ is the specific heat capacity of the solid phase. k_s is the effective axial thermal conductivity of the bulk solid phase. H_i denotes the enthalpy [J kg^{-1}] of the ith pseudospecies. Moreover, the term q_{sg} denotes the solid-gas heat transfer, and q_{sw} denotes the solid-wall heat transfer.

- Gas-phase enthalpy conservation:

$$\frac{d}{dz}(\Phi_s c_{p,g} T_g) = \frac{d}{dz}\left(k_g \frac{dT_g}{dz}\right) + q_{sg} - q_{gw}.$$

Here, $c_{p,g}$ is the specific heat capacity of the gas phase. K_g is the effective axial thermal conductivity of the bulk gas phase. Moreover, the term q_{gw} denotes the gas-wall heat transfer.

- Axial heat conduction within the wall

$$0 = \frac{d}{dz}\left(k_{wall} \frac{dT_{wall}}{dz}\right) + q_{sw} + q_{gw} - q_{wa}.$$

Here, k_{wall} is the axial thermal conductivity of the wall material (in this case, stainless steel 304), and q_{wa} is the heat transfer term between the wall and the outside ambient.

In these constitutive equations above, there are three classes of unknowns: generation rates (r_i), thermochemistry (H_i), bulk effective thermal conductivity (all the k terms), and heat transfer mechanisms (all the q terms). In the sections below, we will describe submodels that we implemented to clarify these different terms in the torrefaction regime.

2.2. Species rate submodel

In the constitutive equations above, the terms r_i relating to the volumetric creation/destruction rate of the ith species are given by the chemical pseudo-processes described in Bates and Ghoniem (2012) [12], giving us the following rate equations for raw biomass (A), solid torrefied pseudospecies B, solid torrefied pseudospecies C, volatile pseudospecies V1, and volatile pseudospecies V2:

$$r_A = -2.48 \times 10^4 \exp(-75976/RT)\rho_A$$

$$r_{V1} = 3.23 \times 10^7 \exp(-75976/RT)\rho_A$$

$$r_{V2} = 1.59 \times 10^{10} \exp(-151711/RT)\rho_B$$

$$r_C = 1.1 \times 10^{10} \exp(-151711/RT)\rho_B$$

$$r_B = -r_A - r_{V2} - r_C$$

Now, to account for moisture, we use a one-step drying mechanism where the original moisture content bound to the biomass (MB) becomes unbound (M) during drying [13]:

$$MB_{(s)} \rightarrow M_{(g)}$$

Her we assume that at any point during the drying and torrefaction process, some moisture content ρ_{MB} is bound to the solid biomass, and that at a certain rate, it irreversibly evaporates from the biomass to become gaseous unbound moisture ρ_M. There are different approaches for modeling this moisture evaporation process. For example, a one-step lump-sum Arrhenius process was given in Peters and Bruch (2003) [13]. However, the approach that we take is different, based on the gasifier modeling approach proposed by Hobbs et al. (1993) and Di Blasi (2004) [3,4]. In this model, the rate of moisture evaporation (the rate r_M at which bound moisture MB turns into unbound moisture M) is assumed to be diffusion controlled:

$$r_M = -r_{MB} = \nu_p A_p k_m (\rho_v - \rho_M),$$

where ν_p is the volumetric biomass particle density number, A_p the average surface area of a biomass particle, ρ_v is the saturation gas-phase moisture density given by the Clausius-Claperyon relation [5]:

$$\rho_v = MW_{H_2O} \exp(12.61 - 4690/T)/RT,$$

and k_m, the solid-gas mass transfer coefficient, is given by

$$k_m = \begin{cases} 2.06\Phi_g Re^{-0.575} Sc^{-2/3}/\varepsilon\rho_g, & k_m < 0.15 \text{ m/s} \\ 0.15, & k_m \ge 0.15 \text{ m/s} \end{cases}.$$

2.3. Reaction thermochemistry submodel

In order to evaluate the H_i terms for the solid and gas pseudospecies, we utilized the same approach described in Bates and Ghoniem (2013) [14].

2.4. Bulk effective thermal conductivity

There are three thermal conductivity constants that we will need to clarify: that of the wall k_{wall}, the bulk solid phase k_s, and the bulk gas phase k_g in the moving bed. As our test reactor's wall is made of stainless steel 304, we utilize the empirical correlation for this material, $k_{wall} = 14.7 + 1.27 \times 10^{-2} (T_{wall} - 273.15)$ [15], where T_{wall} is the wall temperature in Kelvins.

For the bulk solid phase thermal conductivity in the axial direction, we assume that a single number k_s can encapsulate a complex interplay amongst different solid heat transfer mechanisms such as particle-to-particle contact conduction, radiation, intra-particle conduction, and so forth. Recent literature for modeling moving bed biomass gasifiers generally utilizes empirical correlation such as Di Blasi (2013) [6]:

$$k_s = 0.0013 + 0.005\left(\frac{T_s}{1000}\right) + 0.63\left(\frac{T_s}{1000}\right)^2.$$

Likewise, the effective bulk gas-phase is given by Ref. [6]:

$$k_g = 4.8 \times 10^{-4} T_g^{0.716}.$$

2.5. Heat transfer mechanisms

The energy balance equations described above call for various heat transfer mechanisms: between the solid and the gas (q_{sg}), between solid and the wall (q_{sw}), between gas and the wall (q_{gw}), and between wall and the external ambient (q_{wa}). In this section, we will describe the different terms accordingly.

Solid-gas heat transfer. The volumetric heat flow rate q_{sg} (in units of W m^{-3}) from the solid to the gas phase is generally given in the following form:

$$q_{sg} = \nu_p A_p (1-\varepsilon)\gamma h_{sg}(T_s - T_g),$$

where ν_p is the particle density number [m^{-3}], A_p is the particle surface area [m^2], and γ is an adjustable factor proposed by Hobbs et al. [2] and later generalized by Di Blasi [7] to account for unsteady heat transfer and chemical reactivity effects. The magnitude of this adjustable factor ranges from 0.02 to 1 in the biomass gasification and combustion literature. The remaining unknown, h_{sg}, is the solid-gas heat transfer coefficient. Considerable characterization of this heat transfer coefficient has been carried out in biomass moving bed and fluidized bed by prior studies [16–18]. Ultimately, we used the amended correlation proposed by Gupta and Thodos [19], which has been experimentally confirmed with beds of spheres, and has been widely used in other biomass moving bed gasifier models [4,8]:

$$h_{sg} = \frac{2.06 c_{p,g}\rho_g v_g}{\varepsilon}(\mathrm{Re})^{-0.575}(\mathrm{Pr})^{-2/3},$$

where $c_{p,g}$, ρ_g, v_g, and ε are the specific heat capacity, mass density, superficial axial velocity of the gas phase, and void fraction in the moving bed, respectively. In the expression above, $\mathrm{Re} = d_p v_g/\nu_g$ and $\mathrm{Pr} = c_{pg}\mu_g/k_g$ are the Reynolds and Prandtl numbers associated with the superficial flow of the gaseous phase in the moving bed, respectively.

Gas-wall and solid-wall heat transfer. We can write the volumetric heat flow rate [W m^{-3}] due to heat loss from the gas phase to the wall (q_{gw}) and from the solid phase to the wall (q_{sw}) as:

$$q_{gw} = \frac{2h_{gw}}{R_r}(T_g - T_{wall}).$$

$$q_{sw} = \frac{2h_{sw}}{R_r}(T_s - T_{wall}).$$

In order to calculate the gas-wall heat transfer coefficient h_{gw}, first an overall effective moving bed-to-wall convective heat transfer coefficient h_w is defined [20]:

$$h_w = 0.96 k_r^0 R_r^{-4/3} + 0.033 k_g(\mathrm{Pr})(\mathrm{Re}) d_p^{-1},$$

where k_r^0 is the static effective thermal conductivity in the *radial* direction of the moving bed, defined by Ref. [20] in Table S1 in the Supplemental section. If we imagine that the biomass moving bed is defined by a different bulk effective thermal conductivity in the *radial* direction for the solid phase k_{rs} and the gas phase k_{rg} (these values may be different from the axial thermal conductivity values k_s and k_g), then, we can express the gas-to-wall heat transfer coefficient as a component of the overall effective moving bed-to-wall heat transfer coefficient h_w [21]:

$$h_{gw} = \frac{k_{rg}}{k_{rg}+k_{rs}} h_w.$$

By the same reasoning, for the solid phase, we can define a solid-to-wall convective heat transfer coefficient h_{sw} as a component of h_w [21]:

$$h_{sw} = \frac{k_{rs}}{k_{rg}+k_{rs}} h_w.$$

Wall-ambient heat transfer. We can write the volumetric heat flow rate q_{wa} [W m^{-3}] due to heat loss from the wall at temperature T_{wall} to the ambient at room temperature in the form:

$$q_{wa} = \frac{2h_{wa}}{R_m}(T_{wall} - T_{amb}),$$

where the effective wall-to-ambient heat transfer coefficient h_{wa} is defined as a combination of heat transfer through the metallic wall of thickness $R_m - R_r$, through the outer insulation layer of thickness $R_w - R_m$, and of the heat transfer between the ambient air and the outer surface of the reactor system at R_w:

$$h_{wa} = \frac{1}{2R_r - R_m}\left(\frac{\ln(R_m/R_r)}{k_{wall}} + \frac{\ln(R_w/R_m)}{k_{ins}} + \frac{1}{R_w h_{air}}\right)^{-1},$$

where $k_{ins} = 0.0159\,\mathrm{W\,m^{-1}\,K^{-1}}$ is the thermal conductivity of the insulating material (in the case of our laboratory-scale reactor, this material comprises of aluminum silica, McMaster-Carr 93315K71), and where $h_{air} = 10\,\mathrm{W\,m^{-2}\,K^{-1}}$ is the heat transfer coefficient in static air at room temperature.

2.6. Oxidation model

After air enters at the bottom of the reactor ($z = L_r$), we assume that the oxidation reaction with the volatile species and the torrefied biomass is very rapid, occurring at the bottommost part of the reactor with a negligible reaction zone thickness. This oxidative reaction is assumed to act on a small fraction θ_V of the volatile gas released (of characteristic molecular composition CH_xO_y) at the very bottom of the reactor, burning it to completion in a one-step irreversible reaction:

$$CH_xO_y + (1 + 0.25x - 0.5y)(O_2 + 3.76N_2) \rightarrow CO_2 + 0.5x\,H_2O + 3.76 \times (1 + 0.25x - 0.5y)\,N_2$$

This simplified one-step reaction likely does not reflect the actual complex set of reactions occurring within the reaction zone, such as the production of CO and other species. In a subsequent study, this reaction can be refined to produce fine-grained results. However, given that in this study, we are less interested in the precise gaseous composition and more in the overall energy balance of the system, we deem that this simplified approach will yield predictive results while keeping the overall model computation time reasonable.

In order to estimate the chemical compositions of the volatile pseudospecies V1 and V2, we use the experimentally fitted results from Bates and Ghoniem (2012) [12] reproduced in Supplemental Table S2. The composite higher heating value HHV_V of the volatiles is also provided in Bates and Ghoniem (2013) [14]. Therefore, the flux of energy release [W m^{-2}] from volatile combustion, when measured under standard conditions of formation, is given as $\theta_V\ \Phi_{Vol}\ HHV_V$, where $\Phi_{Vol} = \Phi_{V1}(z = L_r) + \Phi_{V2}(z = L_r)$.

After the incoming air combusts the volatile gases, we expect that any excess air will also react with a fraction θ_B of the exiting torrefied biomass (of characteristic molecular composition CH_aO_b, with a and b determined by the final solid elemental composition at $z = L_r$). The oxidation reaction is once again assumed to be irreversible one-step:

$$CH_aO_b + (1 + 0.25a - 0.5b)(O_2 + 3.76N_2) \rightarrow CO_2 + 0.5a\,H_2O + 3.76 \times (1 + 0.25a - 0.5b)\,N_2$$

The higher-heating value HHV_B of oxidizing the torrefied biomass can be inferred from the Boie Equation (1953) [22] as a function of the elemental composition (Y_C, Y_H, Y_O, and Y_N) of the torrefied biomass:

$$HHV_B\ [\mathrm{J\ kg^{-1}}] = 1000 \times (351.69\ Y_C + 1162.46\ Y_H - 110.95 Y_O + 62.8\ Y_N)$$

Therefore, the flux of energy release [W m^{-2}] from the combustion of torrefied biomass, when measured under standard conditions of formation, is given as $\theta_B\ \Phi_s(z = L_r)\ HHV_B$.

Because we assume that these oxidation reactions occur at the very bottom of the reactor, they enter into the reactor model as boundary

conditions for the energy balance equations at $z = L_r$. For the gas phase, the boundary condition is written as follows:

$$k_g \left.\frac{dT_g}{dz}\right|_{z=L_r} = (1-\varepsilon)\theta_B \Phi_s(L_r)\mathrm{HHV}_B + (1-\varepsilon)\theta_V \Phi_{\mathrm{Vol}}\mathrm{HHV}_V + c_{p,\mathrm{air}}\Phi_{\mathrm{air}}(T_a - T_0) + c_{p,\mathrm{vol}}\Phi_{\mathrm{Vol}}(T_g(L_r) - T_0) - c_{p,\mathrm{flue}}\Phi_{\mathrm{flue}}(T_g(L_r) - T_0) - \eta_{\mathrm{ga}}(T_g(L_r) - T_{\mathrm{amb}}),$$

where T_a is the inlet air temperature. To understand the equation above, we will examine the terms on the right-hand side one by one. The first term relates to the energy from the partial combustion of torrefied biomass. The second term relates to the energy from the combustion of volatile gases. The third term relates to the enthalpy carried by the incoming air with respect to the standard reference temperature T_0. The fourth term relates to the enthalpy carried by the pre-combusted volatile gases at position $z = L_r$. The fifth term relates to the enthalpy carried away by the flue gases (mixture of CO_2, H_2O, and some unburned volatiles). The sixth term relates to the heat loss from the bottom of the reactor to the ambient air in the gas phase, with η_{ga} defined as:

$$\eta_{\mathrm{ga}} = \left(\frac{1}{h_{\mathrm{gw}}} + \frac{R_m - R_r}{k_{\mathrm{wall}}} + \frac{R_w - R_m}{k_{\mathrm{ins}}} + \frac{1}{h_{\mathrm{air}}}\right)^{-1}.$$

Likewise, at the bottom of the reactor, the solid-phase boundary condition is given as:

$$k_s \left.\frac{dT_s}{dz}\right|_{z=L_r} = \varepsilon\theta_B \Phi_s(L_r)\mathrm{HHV}_B + \varepsilon\theta_V \Phi_{\mathrm{Vol}}\mathrm{HHV}_V + c_{p,\mathrm{char}}\Phi_{\mathrm{s}}(L_r)(T_s(L_r) - T_0) - c_{p,\mathrm{char}}\theta_B\Phi_{\mathrm{s}}(L_r)(T_s(L_r) - T_0) - \eta_{\mathrm{sa}}(T_{\mathrm{s}}(L_r) - T_{\mathrm{amb}}).$$

The terms on the right-hand side are interpreted as follows. The first term relates to the energy from the partial combustion of torrefied biomass. The second term relates to the energy from the combustion of volatile gases. The third term relates to the enthalpy carried by the incoming pre-combustion torrefied biomass with respect to the standard reference temperature T_0. The fourth term relates to the enthalpy carried away by the post-combusted torrefied biomass with respect to the standard reference temperature T_0. The fifth term relates to the heat loss from the bottom of the reactor to the ambient air in the solid phase, with η_{sa} defined as:

$$\eta_{\mathrm{sa}} = \left(\frac{1}{h_{\mathrm{sw}}} + \frac{R_m - R_r}{k_{\mathrm{wall}}} + \frac{R_w - R_m}{k_{\mathrm{ins}}} + \frac{1}{h_{\mathrm{air}}}\right)^{-1}.$$

2.7. Initial and boundary conditions

We have already specified two boundary conditions for the solid- and gas-phase energy balance in the previous section. In this section, we specify the other initial and boundary conditions needed to completely define the model.

For solid-phase energy balance, the second boundary condition is specified at reactor inlet $z = 0$, where the raw biomass enters the reactor at room temperature. At the same position, the exact temperature of the outgoing flue gas is unknown, but like other similar biomass gasifier and combustor models [4,23], we impose a convective outflow boundary condition:

$$\left.\frac{dT_g}{dz}\right|_{z=0} = 0.$$

For the energy balance equation governing the wall conduction, at both the top and the bottom of the reactor, there is heat loss from the wall to the surrounding:

$$\left.\frac{dT_{\mathrm{wall}}}{dz}\right|_{z=0} = h_{\mathrm{air}}(T_{\mathrm{wall}} - T_{\mathrm{amb}}),$$

$$\left.\frac{dT_{wall}}{dz}\right|_{z=L_r} = -\frac{(T_{\mathrm{wall}} - T_{\mathrm{amb}})}{\frac{R_m - R_r}{k_{\mathrm{wall}}} + \frac{R_w - R_m}{k_{\mathrm{ins}}} + \frac{1}{h_{\mathrm{air}}}}.$$

The differences in the two boundary conditions above reflect the fact that for our laboratory-scale reactor set-up, the bottom is completely insulated, but the top is not.

For the solid-phase species mass balance equations (A, B, C, and bound moisture), as well as the elemental composition (C, H, O, N, and ash), the initial conditions are given at the top of the reactor $z = 0$ by what is known about the type of biomass, the feeding rate, as well as the laboratory proximate and ultimate analysis results on the raw biomass. These values will be specified for the different experiments that we run below. In contrast, for the gas-phase species mass balance equations (V1, V2, and unbound moisture), the initial conditions are specified at the bottom of the reactor $z = L_r$ by the combustion conditions.

2.8. Solution procedure

The countercurrent flow results in a split-boundary value problem which was solved iteratively, as done previously [9] for implementing a countercurrent biomass gasifier model. We begin the iteration with a guessed temperature profile of the reactor. Then the mass balance and elemental composition equations were solved in MATLAB using a stiff solver (ODE15s). Then to solve the temperature profiles, the reactor was discretized axially, and the second-order differential equations were implemented using the method of lines. The resultant temperature profile solution was then used to solve the mass balance and elemental composition equations, and so on, until the differences in the temperature profiles in subsequent iterations converge to less than 0.01 K.

3. Results

In Part I of the study, we presented four experimental conditions for operating the laboratory-scale reactor, with a radius $R_r = 5.08$ cm and length $L_r = 38.15$ cm. In this section, we will solve the model proposed above to assess the fit with our experimental data. Firstly, Table 1 lists the different experimental parameters used for the four experiments. These values inform the initial conditions of our model.

For each of the four experimental set-ups, the model was solved for the gas-phase (solid blue lines in Fig. 3), solid-phase (red dashed lines),

Table 1
Input parameters for the model.

Parameter	Experiment #1	Experiment #2	Experiment #3	Experiment #4
Biomass type	Pine shavings	Pine shavings	Pine shavings	Rice husks
Bulk density	30 kg m^{-3}	30 kg m^{-3}	30 kg m^{-3}	100 kg m^{-3}
Particle dimensions	11 × 6 × 0.2 (mm) (sheet)	11 × 6 × 0.2 (mm) (sheet)	11 × 6 × 0.2 (mm) (sheet)	8 × 2 × 2 (mm) (ellipsoid)
Biomass flux	0.014 kg m^{-2} s^{-1}	0.014 kg m^{-2} s^{-1}	0.004 kg m^{-2} s^{-1}	0.020 kg m^{-2} s^{-1}
Air mass flux	0.017 kg m^{-2} s^{-1}	0.027 kg m^{-2} s^{-1}	0.010 kg m^{-2} s^{-1}	0.018 kg m^{-2} s^{-1}
Ash content	1.6%	1.6%	1.6%	17%
Formula	$CH_{1.36}O_{0.68}$	$CH_{1.36}O_{0.68}$	$CH_{1.36}O_{0.68}$	$CH_{1.23}O_{1.16}$

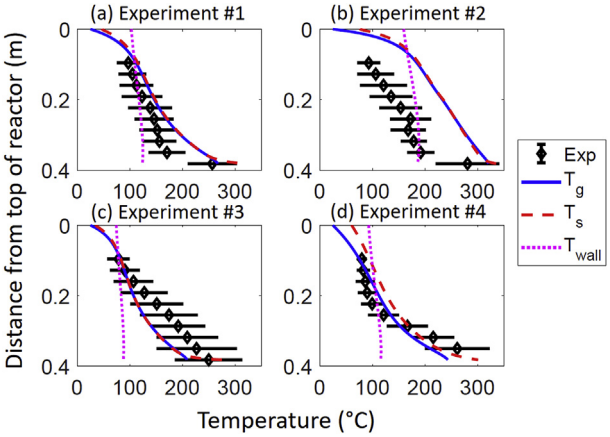

Fig. 3. Axial steady-state temperature profiles for simulated gas phase (blue solid line), simulated solid phase (red dashed line), and simulated wall temperature (purple dotted line) in the biomass torrefaction reactor as compared to that measured on a profile thermocouple (black open diamonds with error bars) in our experimental set-up. (For interpretation of the references to colour in this figure legend, the reader is referred to the Web version of this article.)

and wall (magenta dotted lines) temperature profiles. As can be seen, in most cases, the model has a reasonable fit with the experimental data (open black diamonds with horizontal error bars).

In the case of pine shavings, the modeled solid-phase temperature is almost identical to the modeled gas-phase temperature, but in the case of rice husks, possibly due to the larger thickness of the biomass particles and the longer time for interior thermal conduction within the solid particles, the modeled solid-phase temperature lags by about 10–20K. However, in all four cases, it was experimentally demonstrated that the measured and modeled solid phase successfully reached torrefaction conditions ($> 200\,^{\circ}C$) under steady state. As we increase the air mass flux while keeping the solid mass flux constant (comparing Expt. #2 to Expt. #1), we see that the modeled solid and gas phases reach higher temperatures. As we decrease the incoming biomass mass flux relative to the air mass flux (comparing Expt. #3 to Expt. #1), the modeled temperature profile in Expt. #3 becomes more linear as the relatively weaker downward solid advection allows the countercurrent upward gas advection to deposit more heat further up the moving bed. This also increases the width of the reaction zone, and hence, the solid residence time. Finally, as we switch from pine shavings to the rice husks (comparing Expt. #4 to Expt. #1), we observe that the modeled temperature profile becomes sharper at the bottom of the reactor, as more heat from the gas is deposited to the denser rice husks near the bottom of the reactor.

For most of the experiments (#1, #3, and #4), there seems to be a reasonable fit between the measured and modeled temperature profiles in the biomass reactor. For experiment #2, while the modeled temperature profiles resemble the shape and slope of the measured profile, they are displaced about 50° higher, and therefore do not represent as good of a fit as those from the other experiments. One possible reason for this is that the chemical kinetics model developed by Bates and Ghoniem [12] is mostly derived from mild torrefaction data and best represents the lower range of reaction temperatures. In Experiment #2, as the maximum temperature inside the reactor approaches 300 °C, the reaction gradually transitions from biomass torrefaction into pyrolysis. This also corresponds to Bates and Ghoniem's observation [14] that around this temperature, torrefaction transitions from a net endothermic reaction to a net exothermic one. The researchers posit that this transition represents one of the largest uncertainties in their thermochemistry model. Given that we utilize a different biomass feedstock (pine shavings) than Bates and Ghoniem's study (willow), it is conceivable that the onset of exothermicity may differ, and this can greatly influence the modeled temperature profile. In this case, a better model-experiment fit may be obtained by developing a more accurate kinetics and thermochemistry model for the specific feedstock (pine shavings) that we have used in our study.

While our experimental apparatus could not measure the wall temperature, by simulating it in our model, we can learn something additional about heat transfer and heat loss. We note that in all four cases, the wall's modeled axial temperature profile is nearly flat, at around 100–150 °C. This tells us three things. Firstly, the thermal conductivity of the reactor wall is high compared to the moving bed, such that there is very little axial temperature inhomogeneity. Secondly, near the top 5–10 cm of the reactor, the modeled wall temperature is significantly higher than the modeled moving bed temperature, suggesting that in addition to gas-phase advection, wall-to-bed heat transfer plays some role in pre-heating the incoming raw biomass. This finding is somewhat surprising and not described, to our knowledge, in any other existing biomass gasifier models. Thirdly, due to the elevated modeled temperature of the wall, a non-trivial amount of heat loss occurs in the radial direction, which is not surprising given the small diameter of our test reactor.

Furthermore, by tracking the mass balance, our model can also predict the solid higher-heating value and the elemental composition. These numbers are given in Table 2 for the four experimental conditions described previously, and compared with experimental data. We see that, as a validation for our mathematical model, most of these simulated predictions are within 20% of the experimentally measured values. The only drastic difference concerns the higher-heating value of the torrefied rice husks in experiment #4. We believe that this anomaly can be attributed to the high ash content of torrefied rice husks; as our model used the empirical Boie equation [22] for HHV prediction, it is likely that this correlation breaks down under the high-ash regime.

4. Scaling behaviors

The mathematical model that we developed is also useful in informing the scaling behaviors of the reactor under different dimensions. As an illustration, our current test reactor is small ($R_r = 5.08$ cm) and has a low biomass throughput (on the order of $1\,kg\,h^{-1}$), but as the reactor size is increased towards a commercial scale, we would like to learn how the reactor may behave differently at the larger scale. If the reactor is scaled up, will the heat loss from the reactor wall becomes

Table 2
Solid elemental analyses and higher heating values for torrefied products from simulation and experiments, given on a dry basis.

	Expt. #1 (Pine)	Expt. #2 (Pine)	Expt. #3 (Pine)	Expt. #4 (Rice)
Carbon: Sim	71.2%	62.8%	55.6%	43.9%
Carbon: Expt	66.4%	58.4%	61.2%	44.0%
Hydrogen: Sim	4.0%	4.9%	5.4%	2.6%
Hydrogen: Expt	4.1%	5.0%	4.0%	1.7%
Oxygen: Sim	24.8%	32.2%	39.0%	53.4%
Oxygen: Expt	29.5%	36.6%	34.8%	54.2%
HHV: Sim	26.1 MJ kg^{-1}	23.7 MJ kg^{-1}	21.1 MJ kg^{-1}	10.2 MJ kg^{-1}
HHV: Expt	27.3 MJ kg^{-1}	25.1 MJ kg^{-1}	23.8 MJ kg^{-1}	17.6 MJ kg^{-1}

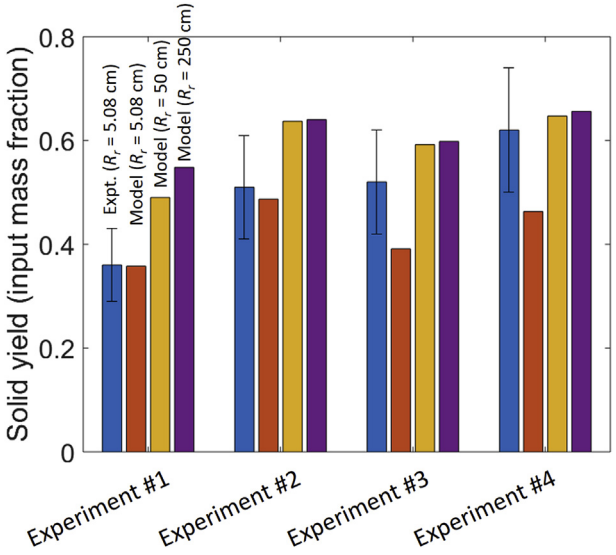

Fig. 4. Mass yields of torrefied solid output (as a measure of reactor performance) for each of the four experiments. The blue bars denote the experimentally measured torrefied solid output mass yield in the laboratory-scale test reactor (Rr = 5.08 cm); the orange bars denote the model predictions for the solid mass yields at the laboratory scale; the yellow bars denote the model predictions for the solid mass yields at a 10x reactor scale-up to achieve the same torrefied output HHV; purple bars denote the model predictions for the solid mass yields at a 50x reactor scale-up to achieve the same torrefied output HHV. (For interpretation of the references to colour in this figure legend, the reader is referred to the Web version of this article.)

less significant? If so, then will the reactor performance improve, under the same torrefaction severity?

To verify this hypothesis, in this section, for each of the four experiments above, we consider two hypothetical cases of scaling the reactor diameter by a factor of 10 and 50. We keep the incoming biomass flux the same, but modulate the incoming air flux such that the scaled-up reactor produces torrefied biomass of the same energy densification (measured in terms of the HHV) as the laboratory-scale reactor. As the incoming air flux is modulated, the meaningful output that measures the reactor performance is the mass yield of the torrefied solid. The implicit assumption here is that, as the reactor is scaled up, the thermochemical reaction and heat transfer conditions within the moving bed remains reasonably invariant.

In Fig. 4 below, for each of the four experimental conditions described above, we plot four torrefied solid output mass yields. The first bars (blue, with the error bars) denote the experimentally determined mass yields in the laboratory-scale reactor, while the second bars (orange) denote the same values predicted by the model run at R_r = 5.08 cm. A comparison between the blue and orange bars show that they generally match, though for some conditions in pine shavings and rice husks, the model tends to under-predict the torrefied solid mass yield compared to the experimental measurement.

The yellow bars and purple bars, on the other hand, respectively, reflect the hypothetical torrefied output solid mass yield as our model is run assuming a 10x and 50x scaled-up reactor, respectively, while maintaining the same higher heating value (HHV) of the output torrefied biomass. In general, the model predicts that for the larger reactor dimensions, the incoming air flux needed to support the same torrefied biomass output HHV is reduced by a factor of around 50% compared to the laboratory-scale reactor. The result manifests in increases in the torrefied solid mass yields by around 10–20%, as the leaner oxygen environment likely consumes a small fraction of the torrefied biomass in the reactor's hot oxidative zone. This predicted increase in the reactor performance is not too surprising, because as the reactor is scaled up, we expect that the relative contribution of heat loss through the side wall diminishes proportionate to $1/R_r$. Therefore, we need to burn less volatiles and torrefied biomass in order to support the same torrefaction condition. This brief analysis demonstrates that our mathematical model is useful in predicting the scaling behaviors of the reactor before we actually build a scaled-up version.

5. Conclusions and discussion

In Part I of this two-part study, we described, analyzed, and experimentally validated a design concept for small-scale, mobile, and decentralized biomass torrefaction reactor operating under oxygen-lean conditions. In this study, we developed a mathematical model (utilizing similar modeling principles in the biomass gasifier literature) to describe our observed experimental results, and interrogate our design concept further under different scaling conditions. We found that at a small laboratory-scale test reactor, heat loss through the side wall is a significant mechanism of heat transfer, and that the metal wall of the reactor also serves as an axial conduit for heat transfer. These are features often not explored in prior biomass gasifier studies, and we contend that the inclusion of these processes into the reactor description will increase the fidelity of the model.

Furthermore, we learned that as we scale up the reactor, we observe an increase in the reactor performance—as measured by the expected mass yield of the torrefied biomass—at the same torrefaction severity (as quantified by the higher heating value of the torrefied biomass). We attributed this to the relative decrease in the amount of heat loss through the walls. These differences illustrate some of the limitations of experimental testing using a small-scale reactor. While for the reason of cost and iterative design, it is likely still preferred for a reactor concept to begin on a small scale initially, our study underscores the importance of understanding and quantifying some of these limitations, as well as predicting any potential differences we may observe as we scale the reactor up.

Furthermore, while our model captures many details of the reactor set-up with reasonable fidelity, we did make various simplifying assumptions along the way. One example is regarding the limited oxidation reaction mechanism that we surmise happens at the bottom of the reactor. As we currently lack a satisfactory solid devolatilization model under the reaction conditions of interest, a more detailed accounting of these phenomena in future studies must first clarify the fundamental thermochemistry and chemical kinetics of oxygen-lean torrefaction. In addition, there were also various quantities, such as the potential thermal gradient in the radial direction, that we were not able to test in our initial experimental set-up. In future studies, a higher-fidelity model representation of the reactor behaviors can be achieved both by measuring these quantities, as well as by developing the mathematical description for these processes.

Finally, the reactor concept presented so far has only undergone preliminary testing and validation, both in terms of the number of experiments performed (4) as well as the amount of detail in the modeling. For our proposed torrefaction reactor design to be useful and scalable, it is necessary to more precisely define the relevant performance metrics—such as energy yield, energy densification, and combustion characteristics—and then more systematically map these performance metrics onto the various reactor operating conditions and biomass types. This mapping will be carried out in a subsequent study in order to demonstrate the robust capability of our reactor design, and to inform an optimization approach.

Acknowledgements

The materials and equipment of work were funded by the MIT Tata Center for Technology and Design. In addition, KSK would like to acknowledge the MIT Tata Center Fellowship, the Dolores Zohrab Liebmann Fellowship, Robert and Patricia Switzer Fellowship, as well as the Legatum Fellowship for supporting his tuition and stipend as a

doctoral student. The authors declare no competing interest.

Appendix A. Supplementary data

Supplementary data to this article can be found online at https://doi.org/10.1016/j.biombioe.2018.12.001.

References

[1] K.S. Kung, Design and Validation of a Decentralized Biomass Torrefaction System, PhD Thesis, Massachusetts Institute of Technology, 2017.
[2] M.L. Hobbs, P.T. Radulovic, L.D. Smoot, Modeling fixed-bed coal gasifiers, AIChE J. 38 (1992) 681.
[3] M.L. Hobbs, P.T. Radulovic, L.D. Smoot, Combustion and gasification of coal in fixed-beds, Prog. Energy Combust. Sci. 19 (1993) 505.
[4] C. Di Blasi, Modeling wood gasification in a countercurrent fixed-bed reactor, AIChE J. 50 (9) (2004) 2306–2319.
[5] A.M. Winslow, Numerical model of coal gasification in a packed bed, Proc. of the 16th Int. Symposium on Combustion, The Combustion Institute, Pittsburg, PA, 1976, p. 503.
[6] C. Di Blasi, C. Branca, Modeling a stratified downdraft wood gasifier with primary and secondary air entry, Fuel 104 (2013) 847–860.
[7] C. Di Blasi, Dynamic behavior of stratified downdraft gasifiers, Chem. Eng. Sci. 55 (2000) 2931–2944.
[8] P.T. Radulovic, M.U. Ghani, L.D. Smoot, An improved model for fixed bed coal combustion and gasification, Fuel 74 (4) (1995) 582–594.
[9] C. Mandl, I. Obernberger, F. Biedermann, Modelling of an updraft fixed-bed gasifier, Fuel 89 (2010) 3795–3806.
[10] J. Ratte, E. Fardet, D. Mateos, J.-S. Hery, Mathematical modelling of a continuous biomass torrefaction reactor: TORSPYD column, Biomass Bioenergy 35 (8) (2011) 3481–3495.
[11] D.A. Granados, P. Basu, F. Chejne, Biomass torrefaction in a two-stage rotary reactor: modeling and experimental validation, Energy Fuels 31 (2017) 5701–5709.
[12] R.B. Bates, A.F. Ghoniem, Biomass torrefaction: modeling of volatile and solid product evolution kinetics, Bioresour. Technol. 124 (2012) 460–469.
[13] B. Peters, C. Bruch, Drying and pyrolysis of wood particles: experiments and simulation, J. Anal. Appl. Pyrol. 70 (2003) 233–250.
[14] R.B. Bates, A.F. Ghoniem, Biomass torrefaction: modeling of reaction thermochemistry, Bioresour. Technol. 134 (2013) 331–340.
[15] R.E. Taylor, H. Groot, J. Ferrier, Thermophysical Properties of SS 304, *TRPL 1904*, Thermophysical Properties Research Laboratory, Purdue University.
[16] T.H. Chilton, A.P. Colburn, Ind. Eng. Chem. 26 (1934) 1183.
[17] B.W. Gamson, G. Thodos, O.A. Hougen, Trans. Am. Inst. Chem. Eng. 39 (1943) 1.
[18] J. De Acetis, G. Thodos, Ind. Eng. Chem. 52 (1960) 1003.
[19] A.S. Gupta, G. Thodos, Direct analogy between mass and heat transfer to beds of spheres, AIChE 9 (6) (1963) 751.
[20] G.F. Froment, K.B. Bischoff, Chemical Reactor Design, Wiley, New York, 1979.
[21] A.P. DeWasch, G.F. Froment, A two-dimensional heterogeneous model for fixed bed catalytic reactors, Chem. Eng. Sci. 26 (1971) 629.
[22] W. Boie, Fuel technology calculations, Energitechnik 3 (1953) 309–316.
[23] J. Cooper, W.L. Hallet, A numerical model for packed-bed combustion of char particles, Chem. Eng. Sci. 55 (2000) 4451.
[24] Kevin S. Kung, Santosh Shanbhogue, Alexander H. Slocum, Ahmed F. Ghoniem, A decentralized biomass torrefaction reactor concept. Part I: multi-scale analysis and initial experimental validation, (2018), https://doi.org/10.1016/j.biombioe.2018.11.004 in this issue.